Redox Biology 24 (2019) 101163

Contents lists available at ScienceDirect

Redox Biology

journal homepage: www.elsevier.com/locate/redox

c-Myc activation promotes cofilin-mediated F-actin cytoskeleton remodeling and telomere homeostasis as a response to oxidant-based DNA damage in medulloblastoma cells

Anna Lewinska[a,*], Jolanta Klukowska-Rötzler[b,c], Anna Deregowska[d], Jagoda Adamczyk-Grochala[a], Maciej Wnuk[d,**]

[a] Department of Cell Biochemistry, Faculty of Biotechnology, University of Rzeszow, Poland
[b] Division of Pediatric Hematology/Oncology, University Hospital, Bern, Switzerland
[c] Department of Emergency Medicine, University Hospital, Bern, Switzerland
[d] Department of Genetics, Faculty of Biotechnology, University of Rzeszow, Pigonia 1, 35-310 Rzeszow, Poland

ARTICLE INFO

Keywords:
Medulloblastoma
c-Myc
Actin
Cofilin
DNA damage
Telomere maintenance

ABSTRACT

Medulloblastoma (MB) is a common and highly aggressive pediatric brain tumor of a heterogeneous nature. According to transcriptome-based profiling, four molecular subgroups of MB have been revealed, namely WNT, SHH, Group 3 and Group 4. High *MYC* mRNA expression and *MYC* gene amplification in MB have been considered as indicators of poor prognosis. However, the role of c-Myc in MB biology is still not well established. In the present study, the effects of c-Myc activation in UW228-MycER MB cell line were investigated using 4-hydroxytamoxifen (4-OHT) induction system. Upon 4-OHT stimulation, an increase in metabolic activity, large-cell/anaplastic (LC/A) phenotype and oxidative stress-mediated DNA damage were observed. However, 53BP1 foci were not implicated in DNA damage response. Instead, cofilin nuclear translocation, changes in F-actin cytoskeleton and the levels of cytoskeletal proteins were shown. Moreover, the telomere length was found to be unaffected that may be associated with the upregulation of TRF proteins. Transcription of nascent RNA (synthesis of new rRNA) and the expression of RNA polymerase I-specific transcription initiation factor RRN3/TIF-IA were also elevated. Moreover, increased levels of DNMT2, a modulator of stress responses, were observed. A small fraction of cells responded differently as oncogene-induced senescence was also noticed. We postulate that c-Myc-mediated modulation of genetic stability of MB cells may trigger cellular heterogeneity and affect adaptive responses to changing environment.

1. Introduction

Medulloblastoma (MB) is a highly aggressive and primitive neuroectodermal pediatric tumor arising in the cerebellum or medulla/brain stem [1]. Despite recent treatment advances, there are still a large number of patients with poor prognosis [2]. This may be partly due to the fact that MB is not a single disease. At least four major molecular subgroups of MB are considered (WNT, SHH, Group 3 and Group 4) that are transcriptionally, genetically, demographically, clinically and prognostically distinct [3–12]. WNT and SHH subgroups have different developmental origin and are characterized by the activation of WNT and SHH signaling pathways, respectively, whereas the cellular origin of Groups 3 and 4 is uncertain and they have overlapping gene expression profiles [3,13,14]. The Group 3 is associated with *MYC* gene amplification and characterized by the highest incidence of metastasis and poor survival among medulloblastomas [3,4]. Thus, it seems worthwhile to study the role of c-Myc in MB biology more detailed.

MYC is considered to be the most frequently amplified oncogene that can promote tumorigenesis in tissues of different origin [15–19]. The elevated expression of its gene product, the transcription factor c-Myc, is associated with poor clinical outcome [20,21]. Increased c-Myc level may be a result of gene amplification, chromosomal translocation, single nucleotide polymorphism in regulatory regions, mutation of upstream signaling pathways and mutations that enhance the stability of the protein [22–25]. c-Myc-mediated oncogenic reprogramming includes growth factor-independent cell proliferation, changes in chromatin structure, ribosome biogenesis, metabolic pathways, cell adhesion, cell size, apoptosis and angiogenesis [22,23,26–31]. c-Myc target

* Corresponding author. Department of Cell Biochemistry, Faculty of Biotechnology, University of Rzeszow, Pigonia 1, 35-310 Rzeszow, Poland.
** Corresponding author.
E-mail addresses: lewinska@ur.edu.pl (A. Lewinska), mwnuk@ur.edu.pl (M. Wnuk).

https://doi.org/10.1016/j.redox.2019.101163
Received 23 February 2019; Accepted 7 March 2019
Available online 13 March 2019

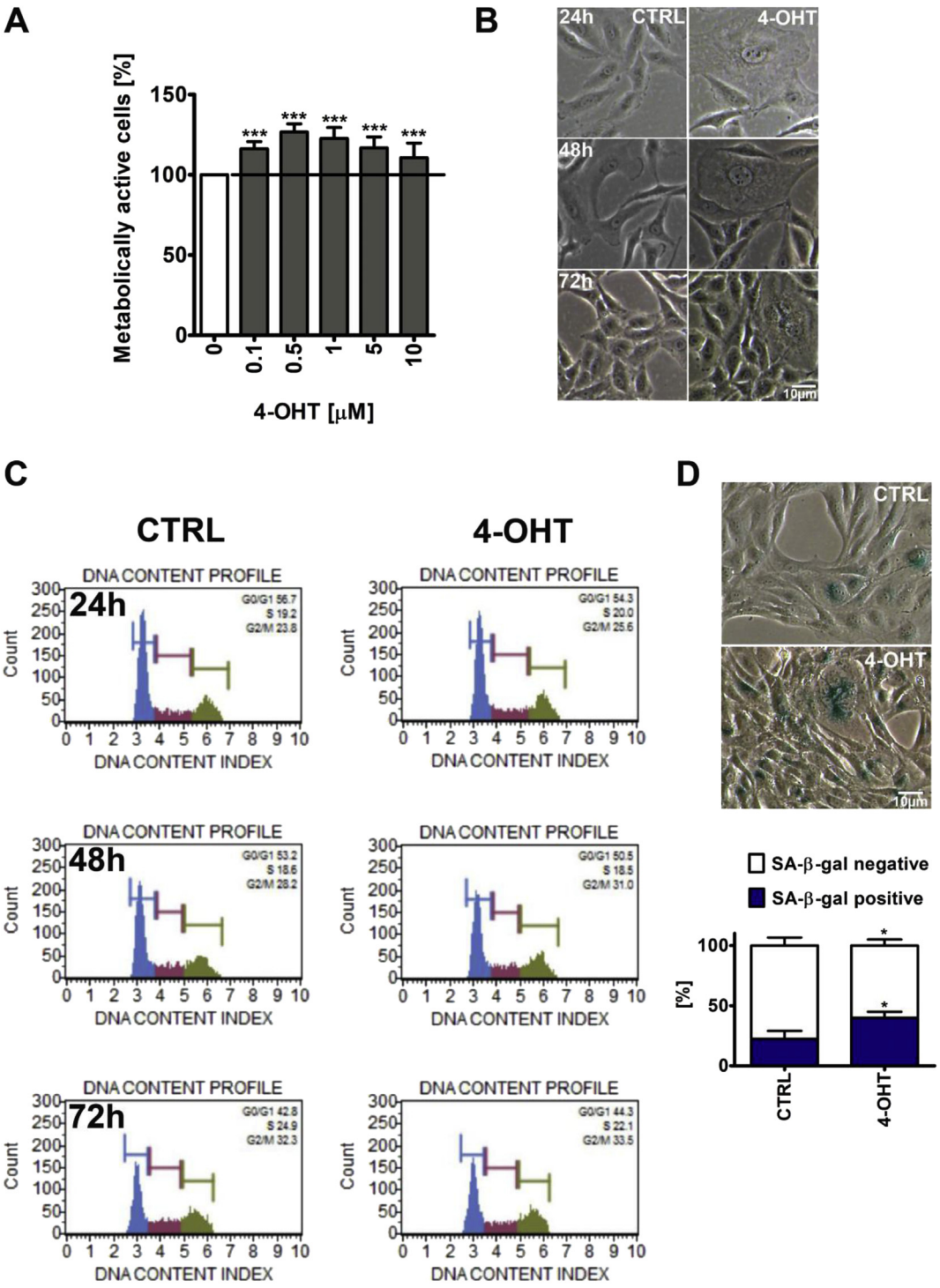

Fig. 1. c-Myc activation-mediated changes in the metabolic activity (A), morphology (B), cell cycle (C) and senescence-associated beta galactosidase (SA-β-gal) activity (D). (A) Metabolic activity reflecting cell viability and cell number was assessed using MTT assay. UW228 MycER cells were stimulated with 0.1–10 μM 4-OHT for 24 h and 0.5 μM concentration was selected for further analysis. To emphasize 4-OHT action, a horizontal line is provided. (B) c-Myc-induced large-cell/anaplastic (LC/A) phenotype as inspected under an inverted microscope after treatment with 0.5 μM 4-OHT for 24, 48 and 72 h. (C) Cell cycle was analyzed using Muse™ Cell Cycle Kit and Muse™ Cell Analyzer after treatment with 0.5 μM 4-OHT for 24, 48 and 72 h. (D) SA- β-gal activity was assayed after 72 h treatment with 0.5 μM 4-OHT and upon 7 days of 4-OHT removal. Bars indicate SD, n = 3, $^{***}p < 0.001$, $^{*}p < 0.05$ compared to the standard growth conditions, CTRL (ANOVA and Dunnett's a posteriori test).

genes have been revealed in a plethora of cancer cells [32–37]. However, it seems that there is no one universal c-Myc target gene network [38]. Thus, c-Myc-associated response may differently modulate tumor cell biology in distinct cancer cells.

In the present study, c-Myc activation-mediated MB cell response was investigated. c-Myc induced a shift in a redox state and genetic instability that promoted actin cytoskeleton remodeling, an increase in the nucleolar activity and TRF2-based telomere homeostasis. On the other hand, some cells were subjected to oncogene-induced cellular senescence that highlight the phenomenon of the heterogeneity of

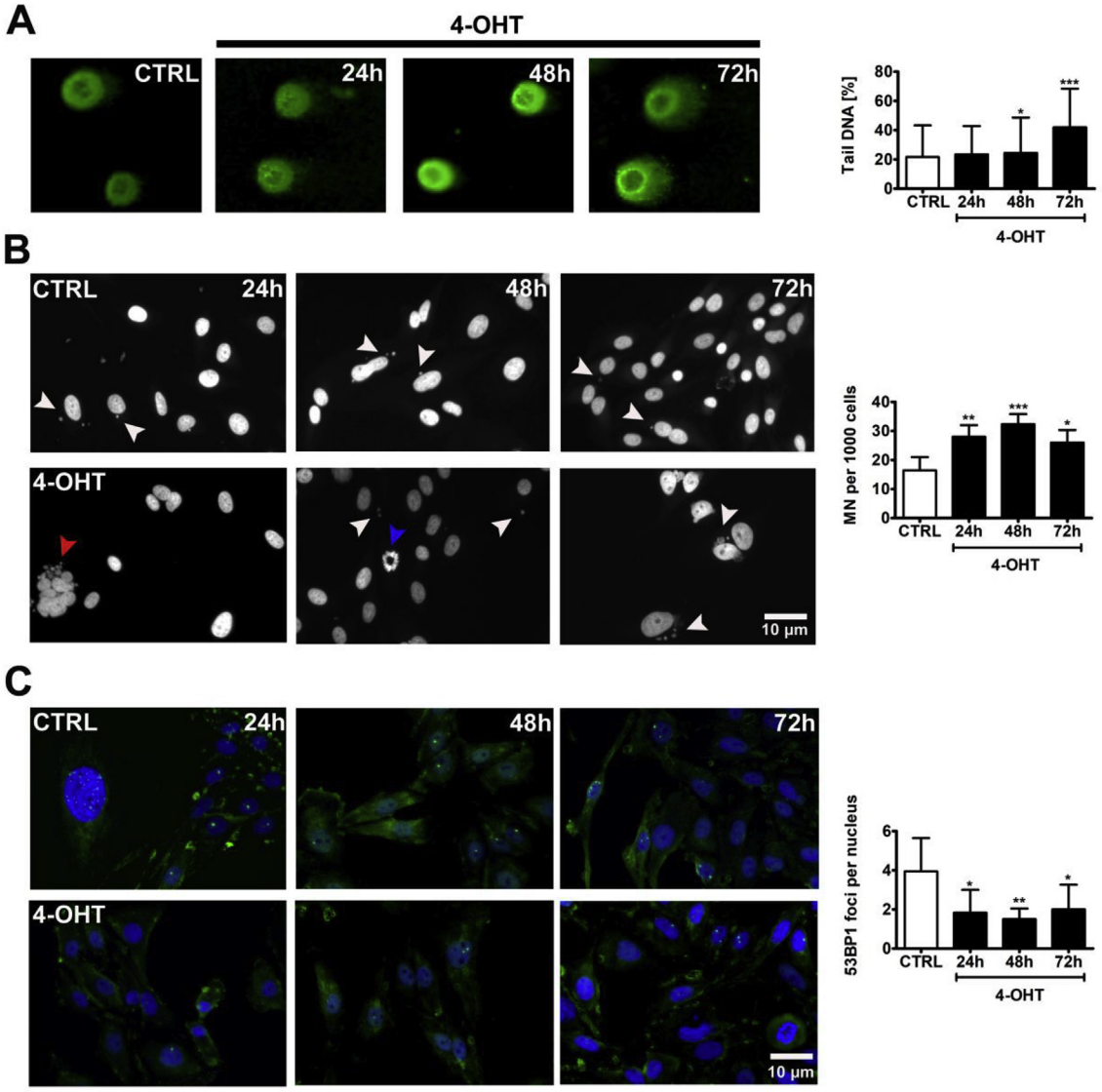

Fig. 2. c-Myc activation-mediated genotoxicity and DNA damage response (DDR). UW228 MycER cells were treated with 0.5 µM 4-OHT for 24, 48 and 72 h. (A) DNA double strand breaks (DSBs) were evaluated using neutral comet assay. DNA was visualized using YOYO-1 staining (green). The percent of tail DNA was used as a parameter of DNA damage. (B) Micronuclei production was assessed using MN assay. White arrowheads indicate micronuclei, whereas red and blue arrowheads show a multinucleated cell and a metaphase spread, respectively. (C) 53BP1 recruitment to sites of DNA damage. 53BP1 foci are presented in green. DNA was visualized using Hoechst 33342 staining (blue). Bars indicate SD, n = 3, $^{***}p < 0.001$, $^{**}p < 0.01$, $^{*}p < 0.05$ compared to the standard growth conditions, CTRL (ANOVA and Dunnett's a posteriori test).

cancer cell populations during adaptations to changing environments.

2. Materials and methods

2.1. Reagents

The reagents, if not otherwise mentioned, were purchased from Sigma-Aldrich (Poznan, Poland) and were of analytical grade.

2.2. Cell culture

The medulloblastoma UW228 cell line expressing tamoxifen-inducible c-Myc-ER was a generous gift from Prof. Alexandre Arcaro (Division of Pediatric Hematology/Oncology, University Hospital, Bern, Switzerland) [39]. UW228 c-Myc-ER cells were cultured in Dulbecco's Modified Eagle Medium (DMEM) supplemented with 10% fetal calf serum (FCS), antibiotic and antimycotic mix solution (100 U/ml penicillin, 0.1 mg/ml streptomycin and 0.25 µg/ml amphotericin B) and selective antibiotic 1 µg/ml puromycin [40]. The cells were grown in a humidified atmosphere at 37 °C and 5% CO_2.

2.3. Metabolic activity, morphology and cell cycle analysis

c-Myc-mediated metabolic activity was evaluated using MTT assay [41] and treatment with 0.1–10 µM 4-hydroxytamoxifen (4-OHT) for 24 h. 4-OHT was dissolved in dimethyl sulfoxide (DMSO) and added to the medium to a given final concentration. The DMSO concentration in the cell culture medium did not exceed 0.1% that did not influence the cell survival. The concentration of 0.5 µM 4-OHT was selected for further analysis on the basis of the most pronounced effect on metabolic activity. After treatment with 0.5 µM 4-OHT for 24, 48 and 72 h, cell morphology was inspected under an inverted microscope and cell cycle analysis was performed using Muse™ Cell Cycle Kit and Muse™ Cell Analyzer according to manufacturer's instructions [41] (Merck Millipore, Warsaw, Poland).

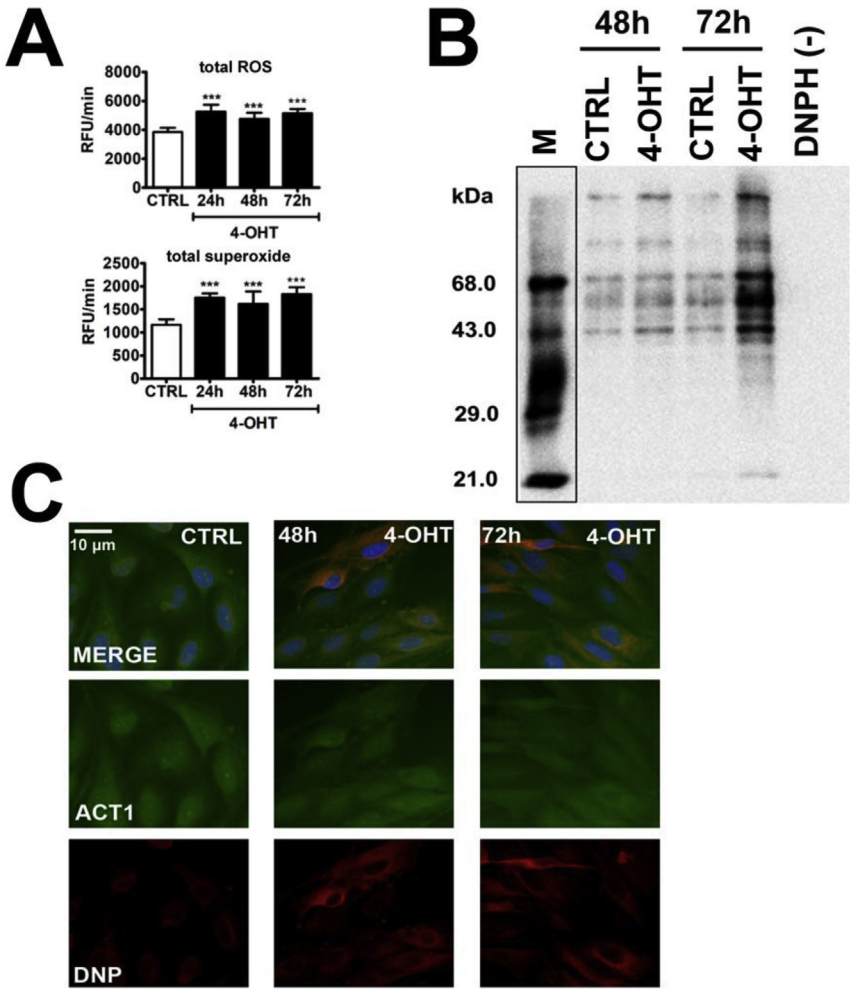

Fig. 3. c-Myc activation-induced oxidative stress. UW228 MycER cells were treated with 0.5 µM 4-OHT for up to 72 h. (A) Intracellular reactive oxygen species (ROS) production and total superoxide production were evaluated using the fluorogenic probes, namely a chloromethyl derivative of H_2DCF-DA (CM-H_2DCF-DA) and dihydroethidium, respectively. Data are presented as relative fluorescence unit per minute (RFU/min). (B) Protein carbonylation was assessed using 2,4-dinitrophenylhydrazine (DNPH) derivatization and anti-DNP antibody. Positive (lane M) and negative (DNPH(−)) controls are also shown. (C) Actin (ACT1) carbonylation. Co-localization analysis of actin immuno-signals (green) with DNP-immuno-signals (red) was performed. DNA was visualized using Hoechst 33342 staining (blue). Bars indicate SD, n = 3, $^{***}p < 0.001$ compared to the standard growth conditions, CTRL (ANOVA and Dunnett's a posteriori test).

2.4. Senescence-associated β-galactosidase activity (SA-β-gal)

UW228 cells were incubated with 0.5 µM 4-OHT for 72 h and SA-β-gal activity was assayed after 7 days of 4-OHT removal [41].

2.5. DNA damage and 53BP1 recruitment

UW228 cells were treated with 0.5 µM 4-OHT for 24, 48 and 72 h. DNA double strand breaks (DSBs) were assessed by neutral single-cell microgel electrophoresis (comet assay) as described elsewhere [41]. The percentage of tail DNA was used as a parameter of DNA damage. Micronuclei production was assayed using a BD™ Gentest Micronucleus Assay Kit following the manufacturer's protocol (BD Biosciences, Poland) [42]. 53BP1 foci were revealed using immunostaining protocol as described elsewhere [42]. Briefly, fixed cells were incubated with the primary antibody anti-53BP1 (1:500, Novus Biologicals, Warsaw, Poland) and the secondary antibody conjugated to FITC (1:1000, Thermo Fisher Scientific, Warsaw, Poland). DNA was visualized using Hoechst 33342 staining. Digital cell images were captured with an In Cell Analyzer 2000 (GE Healthcare, UK) equipped with a high performance CCD camera. 53BP1 foci per nucleus were scored in 200 nuclei.

2.6. Oxidative stress parameters

UW228 cells were treated with 0.5 µM 4-OHT for 24, 48 and 72 h. Intracellular reactive oxygen species (ROS) production and total superoxide production were evaluated using the fluorogenic probes, namely a chloromethyl derivative of H_2DCF-DA (CM-H_2DCF-DA) and dihydroethidium, respectively [43]. Protein carbonylation in the total protein extracts was assayed using an OxyBlot™ Protein Oxidation Detection Kit (Merck Millipore, Warsaw, Poland) using the standard protocol according to the manufacturer's instructions [43]. For each oxyblot analysis, a negative control (no DNPH derivatization) and a positive control with a mixture of standard proteins with attached DNP residues were applied. Actin carbonylation was evaluated using actin and DNP co-immunostaining. Protein derivatization was conducted as described elsewhere [44]. Fixed and derivatized cells were incubated with the primary antibody anti-actin (1:200) and anti-DNP (1:200) (Abcam) and the secondary antibodies conjugated to FITC and TR (1:1000). Digital cell images were captured with an Olympus BX61 fluorescence microscope equipped with a DP72 CCD camera and Olympus CellF software.

2.7. F-actin labeling

UW228 cells were treated with 0.5 µM 4-OHT for 24, 48 and 72 h. Cells were then fixed and stained using Alexa Fluor® 488 Phalloidin (a high-affinity filamentous actin, F-actin, probe conjugated to green-fluorescent Alexa Fluor® 488 dye) [44] according to manufacturer's instructions (Thermo Fisher Scientific).

2.8. Cofilin and fibronectin immunostaining

UW228 cells were treated with 0.5 µM 4-OHT for 24, 48 and 72 h. Cells were fixed and incubated with the primary antibody anti-cofilin (1:200) and anti-fibronectin (1:200) and with the appropriate

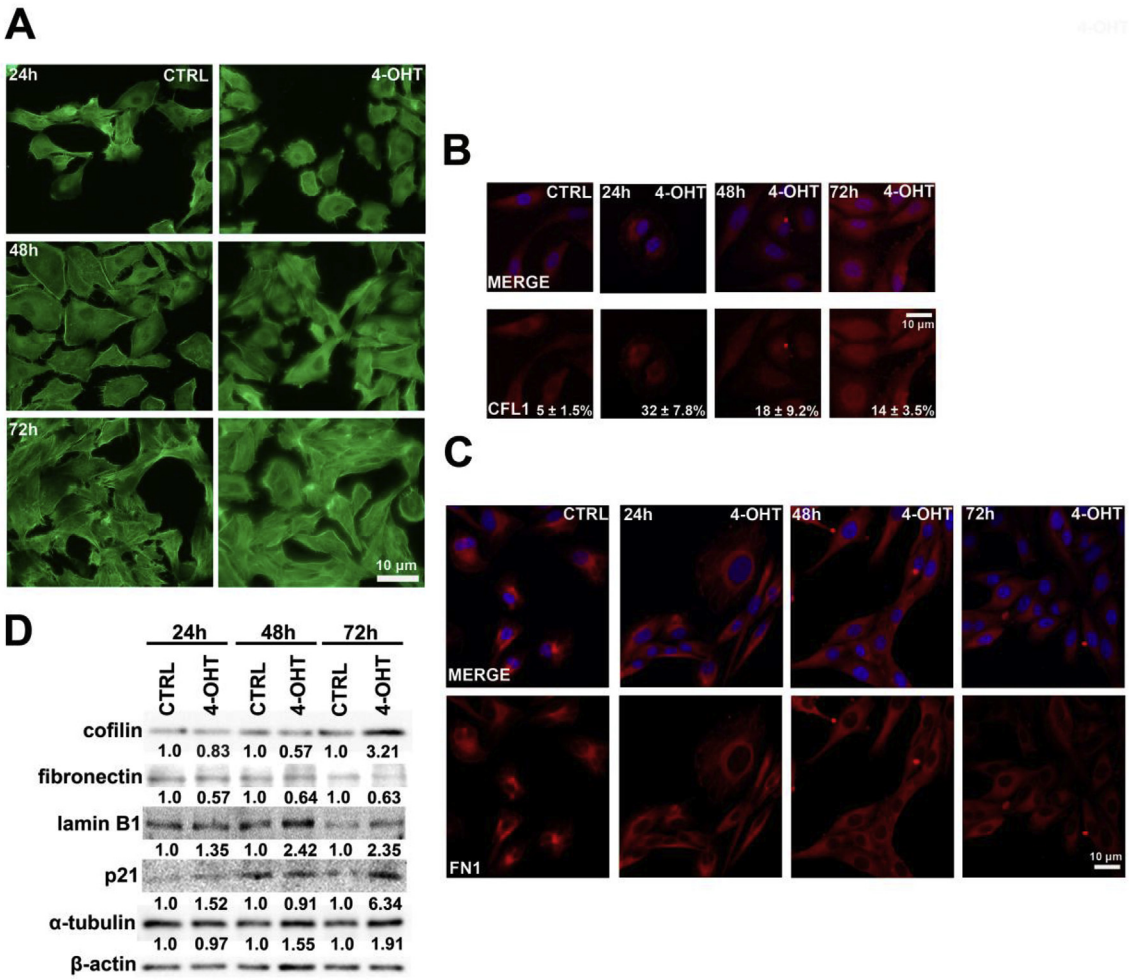

Fig. 4. c-Myc activation-associated changes in the cytoskeleton. UW228 MycER cells were treated with 0.5 μM 4-OHT for up to 72 h. (A) F-actin remodeling. F-actin was visualized using Alexa Fluor® 488 Phalloidin staining (green). (B) Cofilin (CFL1) nuclear translocation. Cofilin was immuno-detected using anti-cofilin antibody (red). DNA was visualized using Hoechst 33342 staining (blue). Nuclear signals of cofilin were quantified [%]. (C) The disruption of fibronectin (FN1) network. Fibronectin was immuno-detected using anti-fibronectin antibody (red). DNA was visualized using Hoechst 33342 staining (blue). (D) WB analysis of cofilin, fibronectin, lamin B1, p21 and α-tubulin protein levels. For the loading control, the antibody against β-actin was used. The data represent the relative density normalized to β-actin.

secondary antibody coupled to TR (1:1000) (Santa Cruz Technology, Abcam, Thermo Fisher Scientific) [44]. Cofilin nuclear signals were scored in 200 cells [%] using ImageJ software and Colocalization plug-in (http://rsb.info.nih.gov/ij/plugins/colocalization.html).

2.9. Western blotting

The total cell protein extracts were prepared as described elsewhere [44]. Polyvinylidene difluoride (PVDF) membrane was incubated with the primary antibody anti-cofilin (1:200), anti-fibronectin (1:400), anti-α-tubulin (1:500), anti-TRF1 (1:1000), anti-TRF2 (1:3000), anti-RRN3 (1:3000), anti-lamin B1 (1:1000), anti-DNMT2 (1:500), anti-p21 (1:100) or anti-β-actin (1:1000) (Abcam, Novus Biologicals, Santa Cruz Technology) and the secondary antibodies conjugated to HRP (1:80000, Sigma-Aldrich). The respective proteins were detected using a Clarity™ Western ECL Blotting Substrate (BioRad, Warsaw, Poland) and a G:BOX imaging system (Syngene, Cambridge, UK) according to the manufacturer's instructions. Densitometry measurements of the bands were performed using GelQuantNET software (http://biochemlabsolutions.com/GelQuantNET.html). The data represent the relative density normalized to β-actin.

2.10. Telomere restriction fragment (TRF) length (Southern blot analysis)

UW228 cells were treated with 0.5 μM 4-OHT for 72 h. TRF length was measured using the TeloTAGGG Telomere Length Assay Kit (Roche, Warsaw, Poland) as described elsewhere [45]. Mean TRF length was calculated using the formula: $L = \Sigma(OD1L1)/\Sigma(OD1)$, where OD1 is the signal intensity at position 1 and L1 is the length of the DNA (bp) at position 1. The OD1 and L1 were estimated using software TotalLab Quant V12.2.

2.11. DNMT2 immunostaining

UW228 cells were treated with 0.5 μM 4-OHT for 24, 48 and 72 h. DNMT2 immunostaining protocol was used as previously described [43].

2.12. Immunodetection of nascent RNA (5-fluorouridine labeling)

UW228 cells were treated with 0.5 μM 4-OHT for 24, 48 and 72 h. Cells were then incubated with a halogenated RNA precursor, 2 mM fluorouridine (FUrd) for 15 min, fixed in 3.7% formaldehyde in PBST (PBS with 0.01% Triton X-100) and incubated with anti-BrdU antibody (1:500, BD Biosciences) followed by incubation with the appropriate

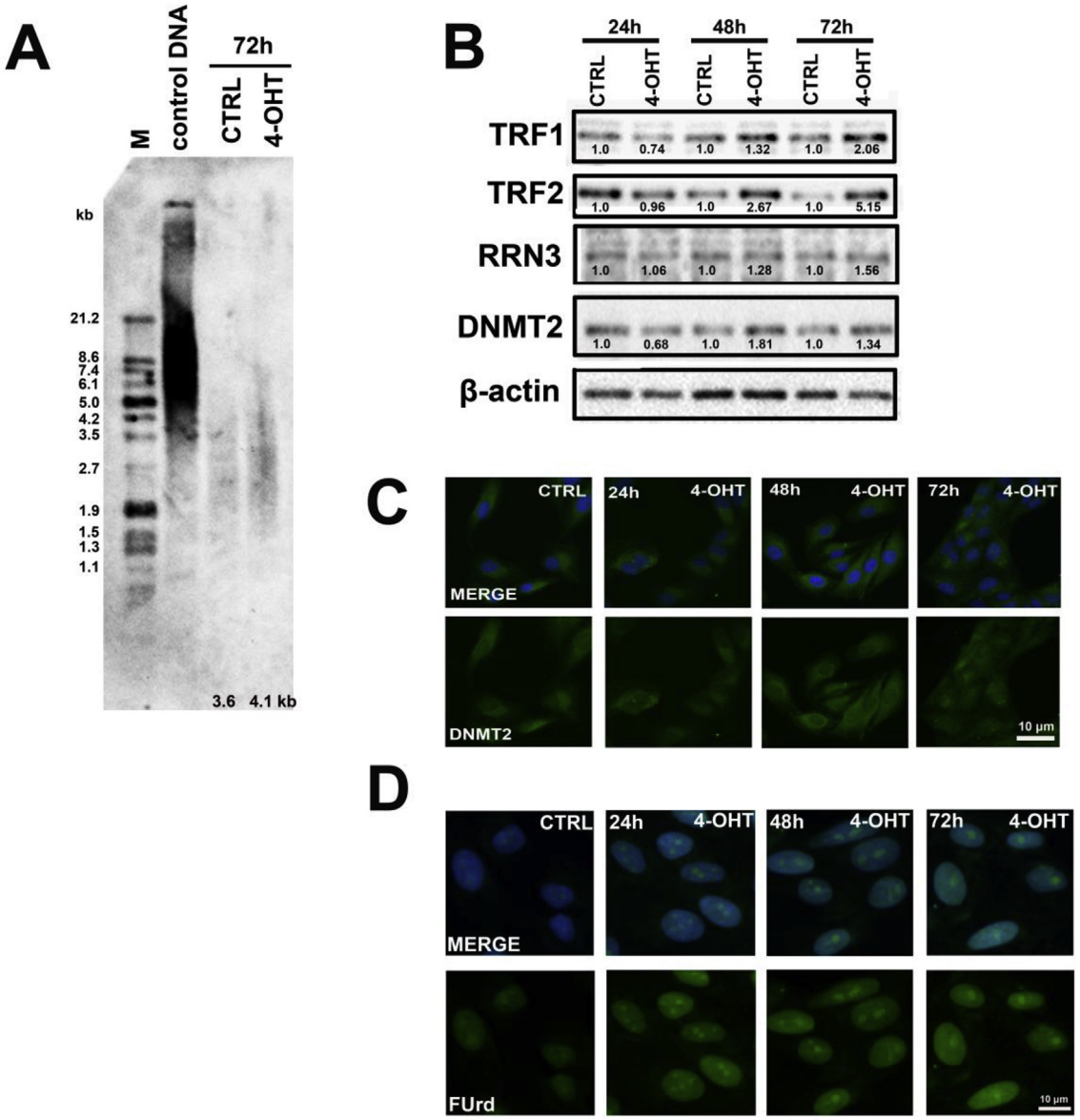

Fig. 5. c-Myc activation-mediated telomere and nucleolus states. UW228 MycER cells were treated with 0.5 μM 4-OHT for up to 72 h. (A) Telomere restriction fragment (TRF) length was estimated using TeloTAGGG Telomere Length Assay Kit. Molecular weight marker and control DNA are also shown. (B) WB analysis of TRF1, TRF2, DNMT2 and RRN3 protein levels. For the loading control, the antibody against β-actin was used. The data represent the relative density normalized to β-actin. (C) DNMT2 immunostaining. DNMT2 was detected using anti-DNMT2 antibody (green). DNA was visualized using Hoechst 33342 staining (blue). (D) Transcriptional activity (new rRNA synthesis) was assessed using FUrd incorporation assay (green). DNA was visualized using Hoechst 33342 staining (blue).

secondary antibody coupled to FITC (1:1000, BD Biosciences) [44].

2.13. Statistical analysis

The results represent the mean ± SD from at least three independent experiments. Statistical significance was assessed by 1-way ANOVA using GraphPad Prism 5, and with the Dunnett's multiple comparison test.

3. Results

3.1. c-Myc-mediated metabolic activity, morphology and cell cycle

c-Myc was activated in the medulloblastoma (MB) UW228-MycER cells by 4-hydroxytamoxifen (4-OHT) stimulation [39] that resulted in increased protein level of c-Myc as already documented [39,46,47]. We tested a range of 4-OHT concentrations that promote an increase in the metabolic activity (MTT assay) and found that 0.5 μM 4-OHT exerted the most accented response after 24 h treatment (Fig. 1 A).

The treatment with 0.5 μM 4-OHT resulted in an increase in metabolic activity of approximately 30% compared to control conditions ($p < 0.001$) (Fig. 1A). Thus, the concentration of 0.5 μM 4-OHT was selected for further analysis. Typically, three time intervals were considered, namely 24, 48 and 72 h of treatment. 4-OHT-mediated changes in the cellular morphology were revealed (Fig. 1B). 4-OHT-treated cells were found to be bigger and more flattened compared to control cells (Fig. 1B) that resemble large-cell/anaplastic (LC/A) phenotype of MB cells with *MYC* gene amplification [3]. c-Myc activation did not result in the changes in the phases of the cell cycle (Fig. 1C). A small fraction of cells responded differently to 4-OHT treatment as oncogene-induced senescence (OIS) was also observed (Fig. 1D). An increase of 17% in the levels of senescence-associated beta-galactosidase positive cells was revealed compared to control conditions ($p < 0.05$) (Fig. 1D).

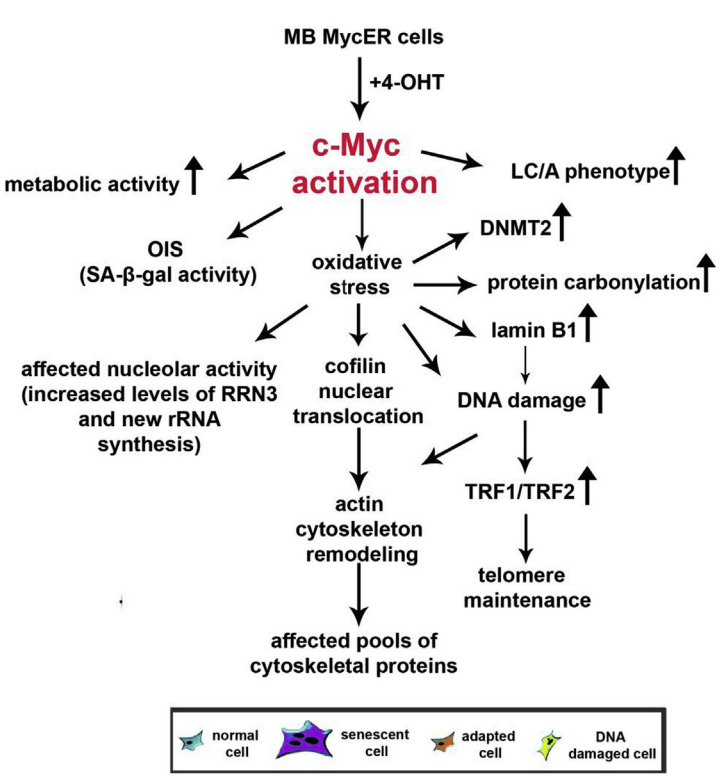

Fig. 6. Pleiotropic effects of c-Myc activation in MB W228 MycER cells. c-Myc activation resulted in redox imbalance that promotes F-actin cytoskeleton reorganization, nuclear translocation of cofilin and changes in the levels of cytoskeletal proteins. Shifts in intracellular redox state also affect lamin B1 pools that may stimulate DNA damage or DNA damage may be accumulated as a result of direct action of reactive oxygen species (ROS). DNA damage induces TRF1-TRF2-based DNA damage response (DDR) that protects telomeres from erosion. Nucleolus state is also affected upon c-Myc activation. Increased transcriptional activity (here new rRNA synthesis) and elevated expression of RNA polymerase I-specific transcription initiation factor RRN3/TIF-IA were observed. c-Myc activation also stimulates DNMT2-based stress response that may protect RNA from degradation. c-Myc activation promotes metabolic activity, but also induces cellular senescence that suggest that c-Myc may provoke cellular heterogeneity as an adaptive response.

3.2. c-Myc-associated oxidant-based genotoxic stress

c-Myc activation induced genotoxicity in MB cells (Fig. 2).

DNA double strand breaks were elevated after 72 h treatment with 4-OHT ($p < 0.001$) (Fig. 2A). A 2-fold increase in the percentage of tail DNA (comet assay) was observed compared to control conditions ($p < 0.001$) (Fig. 2A). Micronuclei formation was the most evident after 48 h treatment ($p < 0.001$) (Fig. 2B). An increase of 80% in micronuclei formation was documented compared to control conditions ($p < 0.001$) (Fig. 2B). However, the accumulation of 53BP1 foci as a part of DNA damage response (DDR) was not shown (Fig. 2C).

We then investigated if c-Myc activation-mediated genotoxicity may be accompanied by oxidative stress. Indeed, the production of total reactive oxygen species (ROS) and total superoxide was increased after 4-OHT stimulation (Fig. 3A).

The disequilibrium of intracellular redox homeostasis (total ROS) was the most evident after 24 h treatment ($p < 0.001$), whereas protein oxidation (here protein carbonylation) was elevated after 72 h treatment (Fig. 3A and B). Actin, a cytoskeletal protein, was found to be carbonylated after prolonged treatment with 4-OHT (Fig. 3C).

3.3. c-Myc-induced F-actin cytoskeleton remodeling

As actin and other cytoskeletal proteins may have a role in cellular stress responses [48], we decided to evaluate 4-OHT-mediated changes in the cytoskeleton of MB cells more detailed (Fig. 4).

We observed c-Myc activation-mediated filamentous actin (F-actin) cytoskeleton remodeling (Fig. 4A) and cofilin nuclear translocation (Fig. 4B). Altered actin dynamics may be a result of p21 upregulation (Fig. 4D). Moreover, a fibrillar fibronectin network was disrupted as after 4-OHT treatment fibronectin signals were dispersed within the whole cytoplasm instead of being concentrated near the nucleus as in the control cells (Fig. 4C). The expression of cytoskeletal proteins was also investigated (Fig. 4D). In general, the expression of cofilin and fibronectin decreased (Fig. 4D). However, after 72 h treatment with 4-OHT, the protein levels of cofilin and α-tubulin increased (Fig. 4D). The protein levels of lamin B1 were also elevated (Fig. 4D). The protein levels of β-actin were almost unchanged (here loading control, Fig. 4D).

3.4. c-Myc-associated changes in the telomeres and nucleolus

As c-Myc activation resulted in genotoxic stress, we investigated then telomere and nucleolus states in 4-OHT-treated MB cells (Fig. 5).

Genotoxic stress did not provoke telomere erosion (Fig. 5A). In contrast, the telomere restriction fragment (TRF) length was unchanged after 4-OHT treatment that may be associated with the upregulation of telomeric repeat binding factor 1 and 2 (TRF1 and TRF2) (Fig. 5B). TRF2-based response was much more pronounced than TRF1-based response (Fig. 5B). As methyltransferase DNMT2 may be implicated in cellular stress responses [43,45], we analyzed the levels and localization of DNMT2 after 4-OHT treatment (Fig. 5B and C). After prolonged treatment (48 and 72 h), the protein levels of DNMT2 were increased (Fig. 5B and C). Moreover, after treatment with 4-OHT for 72 h, DNMT2 was localized in the nucleus (Fig. 5C). Because nucleolus can be also considered to be a stress sensor [49], 4-OHT-mediated nucleolus state was then evaluated (Fig. 5D). We noticed 4-OHT-associated increase in the expression of transcription factor TIF-IA/RRN3 that may modulate the activity of RNA polymerase I (Pol I) (Fig. 5B) and an increase of FUrd-labeled RNA incorporation in nucleoli reflecting the nucleolar transcriptional activity (new rRNA synthesis) (Fig. 5D).

4. Discussion

We present for the first time that c-Myc activation may promote cofilin nuclear translocation and F-actin cytoskeleton remodeling in MB cells that may in turn affect cell division and tumor metastasis. c-Myc-associated redox imbalance may stimulate changes in actin binding and modulating proteins. Cofilin-1 (CFL-1) is a non-muscle isoform of the actin depolymerizing factor (ADF)/cofilin protein family modulating the turnover of actin filaments *in vitro* and *in vivo* [50–52]. Cofilin action resulted in the enhancement of the actin dynamics for cell motility and other physiological functions [53] that is inhibited by the

RhoA–ROCK–LIMK–cofilin pathway [54]. The small GTPase RhoA activates Rho-associated kinase (ROCK), which activates LIM kinase (LIMK), which inhibits cofilin by phosphorylation [54,55]. The components of the RhoA–ROCK–LIMK pathway can be inhibited by the action of different cyclin-dependent kinase (CDK) inhibitors (CKIs), namely p27 inhibits RhoA and p21 inhibits ROCK [56,57]. Thus, the CKI-mediated inhibition of the RhoA–ROCK–LIMK pathway stimulates cofilin-associated cell motility by decreased actin stress fiber and focal-adhesion formation [57]. As c-Myc activation caused an increase in the protein levels of p21 and cofilin, one can speculate that cytoplasmic form of p21 may in turn promote metastatic cancer through regulation of the actin cytoskeleton [57]. More recently, cytoplasmic p21 and p27 function to activate cofilin and increased cofilin expression was found to be associated with breast cancer invasion and metastasis that reflected the oncogenic action of CKIs [58]. Perhaps, c-Myc activation-induced p21 expression in MB cells may also modulate proliferation, migration, invasion and metastasis. Indeed, we have shown that 4-OHT treatment-mediated c-Myc activation resulted in increased metabolic activity (MTT assay) that can indirectly suggest an increase in MB cell number (this study). The levels of other cytoskeletal proteins were also affected after c-Myc activation that may also alter actin dynamics. Moreover, we observed the nuclear translocation of cofilin upon c-Myc activation. Cofilin contains nuclear localization signals (NLS) in its protein sequence that allows for the transport of depolymerized actin to the nucleus [59,60]. Stress stimuli (e.g., heat shock, ATP depletion, DMSO treatment, cytochalasin D or high cytosolic G-actin concentration) induced cofilin-associated actin transition from cytoplasm into nucleus and the formation of cofilin-actin rods [59,61]. The nuclear function of cofilin seems unclear. It has been reported that cofilin is required for RNA polymerase II transcription elongation [62]. Thus, cofilin may regulate transcription and chromatin structure [62]. Indeed, transcriptional activity (new rRNA synthesis) was elevated in c-Myc-activated MB cells that may also reflect increased metabolic activity (this study).

In general, c-Myc activation resulted in intracellular redox disequilibrium as judged by increased production of total reactive oxygen species (ROS) and total superoxide, protein carbonylation and actin carbonylation that may have several effects on MB cell biology (Fig. 6).

The oncogene action itself and/or c-Myc-induced oxidative stress may promote stress-induced premature senescence (SIPS), in particular, oncogene-induced senescence (OIS) (Fig. 6). Indeed, c-Myc activation was accompanied by an increase in the number of senescence-associated beta-galactosidase positive cells. On the other hand, c-Myc activation stimulated metabolic activity. c-Myc-induced changes in lamin B1 levels and DNA damage may be also a result of redox imbalance (Fig. 6). It is also worthwhile to notice that cellular senescence may be accompanied by shifts in lamin B1 pools and genetic instability [63,64]. Lamins may interact with transcription factors and chromatin to regulate transcription. Thus, lamin B1 may have a role in the modulation of oxidative stress response via Oct-1 [65]. Cofilin signaling pathway has been implicated in DNA damage response (DDR) in cancer cells [48]. DNA damage may induce actin reorganization and polymerized actin is required for the repair of DNA double strand breaks (DSBs) [66]. Under DSBs-promoting conditions, ataxia telangiectasia mutated (ATM)-mediated 53BP1, p53 binding protein, recruitment to the sites of DNA damage is observed [67]. However, the formation of 53BP1 foci was not noticed (this study). This may be due to c-Myc-mediated upregulation of telomeric repeat binding factor 1 and 2 (TRF1 and TRF2) protein levels. TRF2 can bind the ATM kinase and inhibit ATM-dependent DDR [68] that can result in limited recruitment of 53BP1 in c-Myc-activated MB cells. TRF1 and TRF2 are multifunctional proteins acting at telomeres in telomere protection, replication, sister resolution and maintenance of length [69]. Perhaps, TRF1 and TRF2 may play a role in the maintenance of telomere homeostasis in c-Myc-activated MB cells as after treatment with 4-OHT, telomere length was found to be unaffected. The upregulation of TRF1 and TRF2 may be also directly related to the action of reactive oxygen species (ROS) [70]. Arsenic trioxide-induced oxidative stress resulted in the upregulation of TRF1 and TRF2 mRNA and protein levels and unaltered telomere length in human gastric cancer MGC-803 cells [70].

c-Myc-induced oxidative stress may also promote DNA methyltransferase 2 (DNMT2)-based adaptive response as a part of the regulatory loop of metabolic pathways through methylation-mediated RNA stabilization [71,72]. Indeed, c-Myc activation resulted in the upregulation of DNMT2 protein levels that may suggest RNA stabilization. More recently, we have shown that DNMT2 may also modulate cell survival and longevity during oxidant-induced senescence in mouse and human fibroblasts [43,45].

As nucleolus is considered to be a stress sensor [49], we investigated c-Myc-mediated nucleolus state in MB cells. c-Myc-induced oxidative stress may modulate the levels of nucleolar proteins, especially these implicated in rRNA synthesis and nucleolar transcriptional activity (new rRNA synthesis) that may also affect cellular homeostasis and genome integrity [28,73].

In conclusion, we found that c-Myc activation in MB MycER cells may have pleiotropic effects on cell biology (Fig. 6). c-Myc induced oxidative stress that resulted in F-actin cytoskeleton remodeling including cofilin nuclear translocation and TRF1-TRF2-based DNA damage response that protected against telomere erosion. c-Myc activation stimulated shifts in the levels of lamin B1 that may have a regulatory role during oxidative stress response but also may induce DNA damage. DNMT2-based response may have a protective effect by RNA stabilization. c-Myc affected nucleolus state by the regulation of rRNA synthesis. Finally, c-Myc may result in elevated metabolic activity, LC/A phenotype or oncogene-induced senescence (Fig. 6). Thus, c-Myc may stimulate different reprogramming modes in MB cells that promotes cellular heterogeneity and emphasizes the importance of customized targeted anti-cancer therapies.

Conflicts of interest

No potential conflicts of interest were disclosed.

Author contributions

Conceived and designed the experiments: MW. Performed the experiments: AL AD JAG MW. Analyzed the data: AL MW. Contributed reagents/materials/analysis tools: AL JKR MW. Wrote the paper: AL.

Acknowledgments

We are indebted to Prof. Alexandre Arcaro (Division of Pediatric Hematology/Oncology, University Hospital, Bern, Switzerland) for sharing with us the medulloblastoma UW228 cell line expressing tamoxifen-inducible c-Myc-ER [39]. This work was partly supported by OPUS 13 Grant number UMO-2017/25/B/NZ2/01983 from National Science Center (Poland).

References

[1] D.N. Louis, H. Ohgaki, O.D. Wiestler, W.K. Cavenee, P.C. Burger, A. Jouvet, B.W. Scheithauer, P. Kleihues, The 2007 WHO classification of tumours of the central nervous system, Acta Neuropathol. 114 (2007) 97–109.

[2] N.U. Gerber, M. Mynarek, K. von Hoff, C. Friedrich, A. Resch, S. Rutkowski, Recent developments and current concepts in medulloblastoma, Cancer Treat Rev. 40 (2014) 356–365.

[3] M.D. Taylor, P.A. Northcott, A. Korshunov, M. Remke, Y.J. Cho, S.C. Clifford, C.G. Eberhart, D.W. Parsons, S. Rutkowski, A. Gajjar, D.W. Ellison, P. Lichter, R.J. Gilbertson, S.L. Pomeroy, M. Kool, S.M. Pfister, Molecular subgroups of medulloblastoma: the current consensus, Acta Neuropathol. 123 (2012) 465–472.

[4] M. Kool, A. Korshunov, M. Remke, D.T. Jones, M. Schlanstein, P.A. Northcott, Y.J. Cho, J. Koster, A. Schouten-van Meeteren, D. van Vuurden, S.C. Clifford, T. Pietsch, A.O. von Bueren, S. Rutkowski, M. McCabe, V.P. Collins, M.L. Backlund, C. Haberler, F. Bourdeaut, O. Delattre, F. Doz, D.W. Ellison, R.J. Gilbertson, S.L. Pomeroy, M.D. Taylor, P. Lichter, S.M. Pfister, Molecular subgroups of

medulloblastoma: an international meta-analysis of transcriptome, genetic aberrations, and clinical data of WNT, SHH, Group 3, and Group 4 medulloblastomas, Acta Neuropathol. 123 (2012) 473–484.
[5] M. Kool, J. Koster, J. Bunt, N.E. Hasselt, A. Lakeman, P. van Sluis, D. Troost, N.S. Meeteren, H.N. Caron, J. Cloos, A. Mrsic, B. Ylstra, W. Grajkowska, W. Hartmann, T. Pietsch, D. Ellison, S.C. Clifford, R. Versteeg, Integrated genomics identifies five medulloblastoma subtypes with distinct genetic profiles, pathway signatures and clinicopathological features, PLoS One 3 (2008) e3088.
[6] P.A. Northcott, D.J. Shih, J. Peacock, L. Garzia, A.S. Morrissy, T. Zichner, A.M. Stutz, A. Korshunov, J. Reimand, S.E. Schumacher, R. Beroukhim, D.W. Ellison, C.R. Marshall, A.C. Lionel, S. Mack, A. Dubuc, Y. Yao, V. Ramaswamy, B. Luu, A. Rolider, F.M. Cavalli, X. Wang, M. Remke, X. Wu, R.Y. Chiu, A. Chu, E. Chuah, R.D. Corbett, G.R. Hoad, S.D. Jackman, Y. Li, A. Lo, K.L. Mungall, K.M. Nip, J.Q. Qian, A.G. Raymond, N.T. Thiessen, R.J. Varhol, I. Birol, R.A. Moore, A.J. Mungall, R. Holt, D. Kawauchi, M.F. Roussel, M. Kool, D.T. Jones, H. Witt, L.A. Fernandez, A.M. Kenney, R.J. Wechsler-Reya, P. Dirks, T. Aviv, W.A. Grajkowska, M. Perek-Polnik, C.C. Haberler, O. Delattre, S.S. Reynaud, F.F. Doz, S.S. Pernet-Fattet, B.K. Cho, S.K. Kim, K.C. Wang, W. Scheurlen, C.G. Eberhart, M. Fevre-Montange, A. Jouvet, I.F. Pollack, X. Fan, K.M. Muraszko, G.Y. Gillespie, C. Di Rocco, L. Massimi, E.M. Michiels, N.K. Kloosterhof, P.J. French, J.M. Kros, J.M. Olson, R.G. Ellenbogen, K. Zitterbart, L. Kren, R.C. Thompson, M.K. Cooper, B. Lach, R.E. McLendon, D.D. Bigner, A. Fontebasso, S. Albrecht, N. Jabado, J.C. Lindsey, S. Bailey, N. Gupta, W.A. Weiss, L. Bognar, A. Klekner, T.E. Van Meter, T. Kumabe, T. Tominaga, S.K. Elbabaa, J.R. Leonard, J.B. Rubin, L.M. Liau, E.G. Van Meir, M. Fouladi, H. Nakamura, G. Cinalli, M. Garami, P. Hauser, A.G. Saad, A. Iolascon, S. Jung, C.G. Carlotti, R. Vibhakar, Y.S. Ra, S. Robinson, M. Zollo, C.C. Faria, J.A. Chan, M.L. Levy, P.H. Sorensen, M. Meyerson, S.L. Pomeroy, Y.J. Cho, G.D. Bader, U. Tabori, C.E. Hawkins, E. Bouffet, S.W. Scherer, J.T. Rutka, D. Malkin, S.C. Clifford, S.J. Jones, J.O. Korbel, S.M. Pfister, M.A. Marra, M.D. Taylor, Subgroup-specific structural variation across 1,000 medulloblastoma genomes, Nature 488 (2012) 49–56.
[7] T.J. Pugh, S.D. Weeraratne, T.C. Archer, D.A. Pomeranz Krummel, D. Auclair, J. Bochicchio, M.O. Carneiro, S.L. Carter, K. Cibulskis, R.L. Erlich, H. Greulich, M.S. Lawrence, N.J. Lennon, A. McKenna, J. Meldrim, A.H. Ramos, M.G. Ross, C. Russ, E. Shefler, A. Sivachenko, B. Sogoloff, P. Stojanov, P. Tamayo, J.P. Mesirov, V. Amani, N. Teider, S. Sengupta, J.P. Francois, P.A. Northcott, M.D. Taylor, F. Yu, G.R. Crabtree, A.G. Kautzman, S.B. Gabriel, G. Getz, N. Jager, D.T. Jones, P. Lichter, S.M. Pfister, T.M. Roberts, M. Meyerson, S.L. Pomeroy, Y.J. Cho, Medulloblastoma exome sequencing uncovers subtype-specific somatic mutations, Nature 488 (2012) 106–110.
[8] G. Robinson, M. Parker, T.A. Kranenburg, C. Lu, X. Chen, L. Ding, T.N. Phoenix, E. Hedlund, L. Wei, X. Zhu, N. Chalhoub, S.J. Baker, R. Huether, R. Kriwacki, N. Curley, R. Thiruvenkatam, J. Wang, G. Wu, M. Rusch, X. Hong, J. Becksfort, P. Gupta, J. Ma, J. Easton, B. Vadodaria, A. Onar-Thomas, T. Lin, S. Li, S. Pounds, S. Paugh, D. Zhao, D. Kawauchi, M.F. Roussel, D. Finkelstein, D.W. Ellison, C.C. Lau, E. Bouffet, T. Hassall, S. Gururangan, R. Cohn, R.S. Fulton, L.L. Fulton, D.J. Dooling, K. Ochoa, A. Gajjar, E.R. Mardis, R.K. Wilson, J.R. Downing, J. Zhang, R.J. Gilbertson, Novel mutations target distinct subgroups of medulloblastoma, Nature 488 (2012) 43–48.
[9] M. Remke, T. Hielscher, A. Korshunov, P.A. Northcott, S. Bender, M. Kool, F. Westermann, A. Benner, H. Cin, M. Ryzhova, D. Sturm, H. Witt, D. Haag, G. Toedt, A. Wittmann, A. Schottler, A.O. von Bueren, A. von Deimling, S. Rutkowski, W. Scheurlen, A.E. Kulozik, M.D. Taylor, P. Lichter, S.M. Pfister, FSTL5 is a marker of poor prognosis in non-WNT/non-SHH medulloblastoma, J. Clin. Oncol. 29 (2011) 3852–3861.
[10] Y.J. Cho, A. Tsherniak, P. Tamayo, S. Santagata, A. Ligon, H. Greulich, R. Berhoukim, V. Amani, L. Goumnerova, C.G. Eberhart, C.C. Lau, J.M. Olson, R.J. Gilbertson, A. Gajjar, O. Delattre, M. Kool, K. Ligon, M. Meyerson, J.P. Mesirov, S.L. Pomeroy, Integrative genomic analysis of medulloblastoma identifies a molecular subgroup that drives poor clinical outcome, J. Clin. Oncol. 29 (2011) 1424–1430.
[11] D.W. Ellison, J. Dalton, M. Kocak, S.L. Nicholson, C. Fraga, G. Neale, A.M. Kenney, D.J. Brat, A. Perry, W.H. Yong, R.E. Taylor, S. Bailey, S.C. Clifford, R.J. Gilbertson, Medulloblastoma: clinicopathological correlates of SHH, WNT, and non-SHH/WNT molecular subgroups, Acta Neuropathol. 121 (2011) 381–396.
[12] E.C. Schwalbe, J.C. Lindsey, S. Nakjang, S. Crosier, A.J. Smith, D. Hicks, G. Rafiee, R.M. Hill, A. Iliasova, T. Stone, B. Pizer, A. Michalski, A. Joshi, S.B. Wharton, T.S. Jacques, S. Bailey, D. Williamson, S.C. Clifford, Novel molecular subgroups for clinical classification and outcome prediction in childhood medulloblastoma: a cohort study, Lancet Oncol. 18 (2017) 958–971.
[13] P. Gibson, Y. Tong, G. Robinson, M.C. Thompson, D.S. Currle, C. Eden, T.A. Kranenburg, T. Hogg, H. Poppleton, J. Martin, D. Finkelstein, S. Pounds, A. Weiss, Z. Patay, M. Scoggins, R. Ogg, Y. Pei, Z.J. Yang, S. Brun, Y. Lee, F. Zindy, J.C. Lindsey, M.M. Taketo, F.A. Boop, R.A. Sanford, A. Gajjar, S.C. Clifford, M.F. Roussel, P.J. McKinnon, D.H. Gutmann, D.W. Ellison, R. Wechsler-Reya, R.J. Gilbertson, Subtypes of medulloblastoma have distinct developmental origins, Nature 468 (2010) 1095–1099.
[14] P.A. Northcott, D.T. Jones, M. Kool, G.W. Robinson, R.J. Gilbertson, Y.J. Cho, S.L. Pomeroy, A. Korshunov, P. Lichter, M.D. Taylor, S.M. Pfister, Medulloblastomics: the end of the beginning, Nat. Rev. Canc. 12 (2012) 818–834.
[15] D.W. Felsher, J.M. Bishop, Reversible tumorigenesis by MYC in hematopoietic lineages, Mol. Cell 4 (1999) 199–207.
[16] I. Flores, D.J. Murphy, L.B. Swigart, U. Knies, G.I. Evan, Defining the temporal requirements for Myc in the progression and maintenance of skin neoplasia, Oncogene 23 (2004) 5923–5930.
[17] M. Jain, C. Arvanitis, K. Chu, W. Dewey, E. Leonhardt, M. Trinh, C.D. Sundberg, J.M. Bishop, D.W. Felsher, Sustained loss of a neoplastic phenotype by brief inactivation of MYC, Science 297 (2002) 102–104.
[18] L. Soucek, J. Whitfield, C.P. Martins, A.J. Finch, D.J. Murphy, N.M. Sodir, A.N. Karnezis, L.B. Swigart, S. Nasi, G.I. Evan, Modelling Myc inhibition as a cancer therapy, Nature 455 (2008) 679–683.
[19] N.M. Sodir, L.B. Swigart, A.N. Karnezis, D. Hanahan, G.I. Evan, L. Soucek, Endogenous Myc maintains the tumor microenvironment, Genes Dev. 25 (2011) 907–916.
[20] R. Beroukhim, C.H. Mermel, D. Porter, G. Wei, S. Raychaudhuri, J. Donovan, J. Barretina, J.S. Boehm, J. Dobson, M. Urashima, K.T. Mc Henry, R.M. Pinchback, A.H. Ligon, Y.J. Cho, L. Haery, H. Greulich, M. Reich, W. Winckler, M.S. Lawrence, B.A. Weir, K.E. Tanaka, D.Y. Chiang, A.J. Bass, A. Loo, C. Hoffman, J. Prensner, T. Liefeld, Q. Gao, D. Yecies, S. Signoretti, E. Maher, F.J. Kaye, H. Sasaki, J.E. Tepper, J.A. Fletcher, J. Tabernero, J. Baselga, M.S. Tsao, F. Demichelis, M.A. Rubin, P.A. Janne, M.J. Daly, C. Nucera, R.L. Levine, B.L. Ebert, S. Gabriel, A.K. Rustgi, C.R. Antonescu, M. Ladanyi, A. Letai, L.A. Garraway, M. Loda, D.G. Beer, L.D. True, A. Okamoto, S.L. Pomeroy, S. Singer, T.R. Golub, E.S. Lander, G. Getz, W.R. Sellers, M. Meyerson, The landscape of somatic copy-number alteration across human cancers, Nature 463 (2010) 899–905.
[21] C.E. Nesbit, J.M. Tersak, E.V. Prochownik, MYC oncogenes and human neoplastic disease, Oncogene 18 (1999) 3004–3016.
[22] M. Eilers, R.N. Eisenman, Myc's broad reach, Genes Dev. 22 (2008) 2755–2766.
[23] N. Meyer, L.Z. Penn, Reflecting on 25 years with MYC, Nat. Rev. Canc. 8 (2008) 976–990.
[24] M.M. Pomerantz, N. Ahmadiyeh, L. Jia, P. Herman, M.P. Verzi, H. Doddapaneni, C.A. Beckwith, J.A. Chan, A. Hills, M. Davis, K. Yao, S.M. Kehoe, H.J. Lenz, C.A. Haiman, C. Yan, B.E. Henderson, B. Frenkel, J. Barretina, A. Bass, J. Tabernero, J. Baselga, M.M. Regan, J.R. Manak, R. Shivdasani, G.A. Coetzee, M.L. Freedman, The 8q24 cancer risk variant rs6983267 shows long-range interaction with MYC in colorectal cancer, Nat. Genet. 41 (2009) 882–884.
[25] J.B. Wright, S.J. Brown, M.D. Cole, Upregulation of c-MYC in cis through a large chromatin loop linked to a cancer risk-associated single-nucleotide polymorphism in colorectal cancer cells, Mol. Cell Biol. 30 (2010) 1411–1420.
[26] C.V. Dang, MYC on the path to cancer, Cell 149 (2012) 22–35.
[27] B. Amati, S.R. Frank, D. Donjerkovic, S. Taubert, Function of the c-Myc oncoprotein in chromatin remodeling and transcription, Biochim. Biophys. Acta 1471 (2001) M135–M145.
[28] M.S. Dai, H. Lu, Crosstalk between c-Myc and ribosome in ribosomal biogenesis and cancer, J. Cell. Biochem. 105 (2008) 670–677.
[29] B. Hoffman, D.A. Liebermann, Apoptotic signaling by c-MYC, Oncogene 27 (2008) 6462–6472.
[30] J. van Riggelen, A. Yetil, D.W. Felsher, MYC as a regulator of ribosome biogenesis and protein synthesis, Nat. Rev. Canc. 10 (2010) 301–309.
[31] C.V. Dang, Rethinking the Warburg effect with Myc micromanaging glutamine metabolism, Cancer Res. 70 (2010) 859–862.
[32] C.V. Dang, K.A. O'Donnell, K.I. Zeller, T. Nguyen, R.C. Osthus, F. Li, The c-Myc target gene network, Semin. Canc. Biol. 16 (2006) 253–264.
[33] H. Ji, G. Wu, X. Zhan, A. Nolan, C. Koh, A. De Marzo, H.M. Doan, J. Fan, C. Cheadle, M. Fallahi, J.L. Cleveland, C.V. Dang, K.I. Zeller, Cell-type independent MYC target genes reveal a primordial signature involved in biomass accumulation, PLoS One 6 (2011) e26057.
[34] Y.H. Kim, L. Girard, C.P. Giacomini, P. Wang, T. Hernandez-Boussard, R. Tibshirani, J.D. Minna, J.R. Pollack, Combined microarray analysis of small cell lung cancer reveals altered apoptotic balance and distinct expression signatures of MYC family gene amplification, Oncogene 25 (2006) 130–138.
[35] I. Schlosser, M. Holzel, R. Hoffmann, H. Burtscher, F. Kohlhuber, M. Schuhmacher, R. Chapman, U.H. Weidle, D. Eick, Dissection of transcriptional programmes in response to serum and c-Myc in a human B-cell line, Oncogene 24 (2005) 520–524.
[36] M. Schuhmacher, F. Kohlhuber, M. Holzel, C. Kaiser, H. Burtscher, M. Jarsch, G.W. Bornkamm, G. Laux, A. Polack, U.H. Weidle, D. Eick, The transcriptional program of a human B cell line in response to Myc, Nucleic Acids Res. 29 (2001) 397–406.
[37] K.I. Zeller, A.G. Jegga, B.J. Aronow, K.A. O'Donnell, C.V. Dang, An integrated database of genes responsive to the Myc oncogenic transcription factor: identification of direct genomic targets, Genome Biol. 4 (2003) R69.
[38] S. Chandriani, E. Frengen, V.H. Cowling, S.A. Pendergrass, C.M. Perou, M.L. Whitfield, M.D. Cole, A core MYC gene expression signature is prominent in basal-like breast cancer but only partially overlaps the core serum response, PLoS One 4 (2009) e6693.
[39] P. Cwiek, Z. Leni, F. Salm, V. Dimitrova, B. Styp-Rekowska, G. Chiriano, M. Carroll, K. Holand, V. Djonov, L. Scapozza, P. Guiry, A. Arcaro, RNA interference screening identifies a novel role for PCTK1/CDK16 in medulloblastoma with c-Myc amplification, Oncotarget 6 (2015) 116–129.
[40] T.D. Littlewood, D.C. Hancock, P.S. Danielian, M.G. Parker, G.I. Evan, A modified oestrogen receptor ligand-binding domain as an improved switch for the regulation of heterologous proteins, Nucleic Acids Res. 23 (1995) 1686–1690.
[41] A. Lewinska, J. Adamczyk-Grochala, A. Deregowska, M. Wnuk, Sulforaphane-induced cell cycle arrest and senescence are accompanied by DNA hypomethylation and changes in microRNA profile in breast cancer cells, Theranostics 7 (2017) 3461–3477.
[42] A. Lewinska, A. Bocian, V. Petrilla, J. Adamczyk-Grochala, K. Szymura, W. Hendzel, E. Kaleniuk, K.K. Hus, M. Petrillova, M. Wnuk, Snake venoms promote stress-induced senescence in human fibroblasts, J. Cell. Physiol. 234 (2019) 6147–6160.
[43] A. Lewinska, J. Adamczyk-Grochala, E. Kwasniewicz, A. Deregowska, E. Semik, T. Zabek, M. Wnuk, Reduced levels of methyltransferase DNMT2 sensitize human fibroblasts to oxidative stress and DNA damage that is accompanied by changes in

proliferation-related miRNA expression, Redox Biol. 14 (2018) 20–34.
[44] A. Lewinska, D. Bednarz, J. Adamczyk-Grochala, M. Wnuk, Phytochemical-induced nucleolar stress results in the inhibition of breast cancer cell proliferation, Redox Biol. 12 (2017) 469–482.
[45] A. Lewinska, J. Adamczyk-Grochala, E. Kwasniewicz, M. Wnuk, Downregulation of methyltransferase Dnmt2 results in condition-dependent telomere shortening and senescence or apoptosis in mouse fibroblasts, J. Cell. Physiol. 232 (2017) 3714–3726.
[46] F. Salm, V. Dimitrova, A.O. von Bueren, P. Cwiek, H. Rehrauer, V. Djonov, P. Anderle, A. Arcaro, The phosphoinositide 3-kinase p110alpha isoform regulates leukemia inhibitory factor receptor expression via c-myc and miR-125b to promote cell proliferation in medulloblastoma, PLoS One 10 (2015) e0123958.
[47] L. Zhou, D. Picard, Y.S. Ra, M. Li, P.A. Northcott, Y. Hu, D. Stearns, C. Hawkins, M.D. Taylor, J. Rutka, S.D. Der, A. Huang, Silencing of thrombospondin-1 is critical for myc-induced metastatic phenotypes in medulloblastoma, Cancer Res. 70 (2010) 8199–8210.
[48] C.Y. Chang, J.D. Leu, Y.J. Lee, The actin depolymerizing factor (ADF)/cofilin signaling pathway and DNA damage responses in cancer, Int. J. Mol. Sci. 16 (2015) 4095–4120.
[49] M.O. Olson, Sensing cellular stress: another new function for the nucleolus? Sci. STKE (2004) 2004:pe10.
[50] J.R. Bamburg, Proteins of the ADF/cofilin family: essential regulators of actin dynamics, Annu. Rev. Cell Dev. Biol. 15 (1999) 185–230.
[51] M.F. Carlier, F. Ressad, D. Pantaloni, Control of actin dynamics in cell motility. Role of ADF/cofilin, J. Biol. Chem. 274 (1999) 33827–33830.
[52] W.A. Elam, H. Kang, E.M. De la Cruz, Biophysics of actin filament severing by cofilin, FEBS Lett. 587 (2013) 1215–1219.
[53] J.J. Bravo-Cordero, M.A. Magalhaes, R.J. Eddy, L. Hodgson, J. Condeelis, Functions of cofilin in cell locomotion and invasion, Nat. Rev. Mol. Cell Biol. 14 (2013) 405–415.
[54] S. Narumiya, M. Tanji, T. Ishizaki, Rho signaling, ROCK and mDia1, in transformation, metastasis and invasion, Cancer Metastasis Rev. 28 (2009) 65–76.
[55] B.W. Bernstein, J.R. Bamburg, ADF/cofilin: a functional node in cell biology, Trends Cell Biol. 20 (2010) 187–195.
[56] A. Besson, S.F. Dowdy, J.M. Roberts, CDK inhibitors: cell cycle regulators and beyond, Dev. Cell 14 (2008) 159–169.
[57] N.G. Starostina, E.T. Kipreos, Multiple degradation pathways regulate versatile CIP/KIP CDK inhibitors, Trends Cell Biol. 22 (2012) 33–41.
[58] W. Wang, R. Eddy, J. Condeelis, The cofilin pathway in breast cancer invasion and metastasis, Nat. Rev. Canc. 7 (2007) 429–440.
[59] H. Abe, R. Nagaoka, T. Obinata, Cytoplasmic localization and nuclear transport of cofilin in cultured myotubes, Exp. Cell Res. 206 (1993) 1–10.
[60] A. Pendleton, B. Pope, A. Weeds, A. Koffer, Latrunculin B or ATP depletion induces cofilin-dependent translocation of actin into nuclei of mast cells, J. Biol. Chem. 278 (2003) 14394–14400.
[61] L.N. Munsie, C.R. Desmond, R. Truant, Cofilin nuclear-cytoplasmic shuttling affects cofilin-actin rod formation during stress, J. Cell Sci. 125 (2012) 3977–3988.
[62] A. Obrdlik, P. Percipalle, The F-actin severing protein cofilin-1 is required for RNA polymerase II transcription elongation, Nucleus 2 (2011) 72–79.
[63] A. Freund, R.M. Laberge, M. Demaria, J. Campisi, Lamin B1 loss is a senescence-associated biomarker, Mol. Biol. Cell 23 (2012) 2066–2075.
[64] E. Sikora, T. Arendt, M. Bennett, M. Narita, Impact of cellular senescence signature on ageing research, Ageing Res. Rev. 10 (2011) 146–152.
[65] A.N. Malhas, C.F. Lee, D.J. Vaux, Lamin B1 controls oxidative stress responses via Oct-1, J. Cell Biol. 184 (2009) 45–55.
[66] C. Andrin, D. McDonald, K.M. Attwood, A. Rodrigue, S. Ghosh, R. Mirzayans, J.Y. Masson, G. Dellaire, M.J. Hendzel, A requirement for polymerized actin in DNA double-strand break repair, Nucleus 3 (2012) 384–395.
[67] G.S. Stewart, Solving the RIDDLE of 53BP1 recruitment to sites of damage, Cell Cycle 8 (2009) 1532–1538.
[68] J. Karlseder, K. Hoke, O.K. Mirzoeva, C. Bakkenist, M.B. Kastan, J.H. Petrini, T. de Lange, The telomeric protein TRF2 binds the ATM kinase and can inhibit the ATM-dependent DNA damage response, PLoS Biol. 2 (2004) E240.
[69] J.R. Walker, X.D. Zhu, Post-translational modifications of TRF1 and TRF2 and their roles in telomere maintenance, Mech. Ageing Dev. 133 (2012) 421–434.
[70] Y. Zhang, E.H. Cao, J.F. Qin, Up-regulation of telomere-binding TRF1, TRF2 related to reactive oxygen species induced by As(2)O(3) in MGC-803 cells, Eur. J. Pharmacol. 516 (2005) 1–9.
[71] M. Schaefer, F. Lyko, Solving the Dnmt2 enigma, Chromosoma 119 (2010) 35–40.
[72] J. Mytych, A. Lewinska, A. Bielak-Zmijewska, W. Grabowska, J. Zebrowski, M. Wnuk, Nanodiamond-mediated impairment of nucleolar activity is accompanied by oxidative stress and DNMT2 upregulation in human cervical carcinoma cells, Chem. Biol. Interact. 220 (2014) 51–63.
[73] I. Grummt, The nucleolus-guardian of cellular homeostasis and genome integrity, Chromosoma 122 (2013) 487–497.